542/0454
Microsystem Technologies 9 (2004) ■■■–■■■ © Springer-Verlag 2004
DOI 10.1007/s00542-004-0454-8

Effects of contact-stress on hot-embossed PMMA microchannel wall profile

K. F. Lei, W. J. Li, Y. Yam

Abstract Hot-embossing (thermal-compression) based microchannel fabrication techniques have gained much attention recently due to their low-cost setup and ease of implementation. However, not much effects have been attempted in trying to understand or characterize the mechanics of the hot-embossing process in fabricating microchannels. Most research groups still rely on trial-and-error processes to hot-emboss microchannels for microfluidic control applications. The present paper describes the application of the contact-stress analysis to understand the mechanism of using molds with micro-features to hot-emboss PMMA substrates. Experimental results showing that the resulting microchannel wall profile can be predicted with good accuracy via a close-form solution of the analysis are also presented.

Key words ■

1
Introduction

Materials such as silicon and glass are excellent choices for low cost manufacturing electronic and mechanical devices. However, they are not suitable for applications in biology and chemistry that involve fluidic devices. This is so because fluidic devices require more surface area than electronic circuits and their interfacing with the external world is more complicated. On the other hand, the most commonly used micromachining methods and materials for fluidic devices, such as silicon etching and single crystalline silicon, are relatively expensive. In the case of a micropump, for example, which normally has a chip size in the order of 1 cm^2 and consists of three or more layers [1], mass fabrication with silicon micromachining is not cost effective at all. Hence, alternate economically viable fabrication method is desired.

Received: 8 August 2003/Accepted: 6 November 2003

K. F. Lei, W. J. Li (✉)
Centre for Micro and Nano Systems, and Department of Automation and Computer-Aided Engineering, The Chinese University of Hong Kong, Shatin, Hong Kong SAR
E-mail: wen@acae.cuhk.edu.hk
Tel.: +852 26098475
Fax: +852 26036002

Y. Yam
Department of Automation and Computer-Aided Engineering, The Chinese University of Hong Kong, Shatin, Hong Kong SAR

Hot-embossing (thermal-compression) based microfluidic device fabrication technique has gained much attention recently due to its low-cost setup and ease of implementation. It is a flexible and low-cost microfabrication method for high aspect ratio polymer based microstructures. By using the electroplated metal mold to "imprint" micro features on polymer substrates, many fully patterned substrates can be produced in a short production cycling time. Many microfluidic devices have already been fabricated by using this technique (e.g., [2, 3]). Depending on the settings, the processes are capable of producing polymer-based channels with widths ranging from a few hundred microns (using SU-8 based electroplated molds) to a few hundred nanometers (using CD based molds), as we have demonstrated recently [4, 5]. In spite of its initial success, however, little has been done in the theory side to understand and to characterize the mechanics of the hot-embossing process in fabricating microstructures. Most research groups still rely on trial-and-error processes to hot-emboss microstructures for microfluidic control applications.

In this paper, we report on our effort to apply contact-stress analysis for the mechanism of using molds with micro-features to hot-emboss polymethylmethacrylate (PMMA) substrates. Both the formulation of analysis and experimental validation are described. The contact-stress analysis appears to serve well in modeling hot-embossing of microchannels on polymer substrates with good prediction of the resulting channel wall profile via a close-form solution.

2
PMMA mechanical analysis

PMMA is a hard, rigid and transparent material at room temperature. Its mechanical, electrical and other properties, however, change significantly with temperature. For normal materials, molecules may occur in three states: solid, liquid and gaseous state, and transitions between these states are sharp. In the case of polymer molecules, however, the situation is much more complicated. In solid state, polymer material is generally in partially or totally amorphous state, purely crystalline structure is only exceptional. A specific amorphous polymer, such as PMMA, can actually exist in a number of states depending on its temperature [6]. As such, a rubbery intermediate zone is often resulted, with no clearly defined melting point. From solid to liquid state of PMMA, two state transitions may be observed: the first is a rigid solid-rubber transition (the transition temperature usually is

5 4 2 | 0 4 5 4 | B
Journal number | Manuscript number
Dispatch: 11.10.2004 Journal: Microsystem Technologies No. of pages: 5
Author's disk received ☑ Used ☑ Corrupted ☐ Mismatch ☐ Keyed ☐

known as glass transition temperature, T_g) and the second is a very indefinite rubber-liquid transition. In solid state (room temperature), PMMA is hard, rigid and transparent. Because of its glass-like appearance, sometimes it is referred to as the glassy state. At this state, molecular movements, other than bond vibrations, are very limited. However, when the temperature is above the glass transition temperature, molecular movements become possible because of acquiring more energy. Because of this phenomenon, if a specimen is heated to a temperature above its glass transition point and then subjected to a tensile stress. The molecules will tend to align themselves in the general direction of the stress. If the mass is then cooled below its transition temperature while the molecule is still under stress, the molecules will become frozen whilst in an oriented state.

The above properties of PMMA possibly explain the physical phenomenon that occurs when the hot-embossing process is applied on PMMA substrate, which is due to localized deformation and re-solidification of the substrate. Furthermore, we desire a quantitative explanation on the geometry of the localized deformation after the hot-embossing process. To derive such mechanical model of a heated mold compressed onto a heated PMMA substrate, Hooke's law for stress-strain relationship is used to model the cross sectional displacement profile of the substrate surface. As will be discussed in the next section, this stress-strain relationship depends on the Young's modulus (which varies with temperature) the Poisson ratio (assumed independent of temperature, $\nu = 0.4$), the channel mold feature width, the temperature of the PMMA, and the pressure applied onto the PMMA by the mold. To determine the temperature dependence of Young's modulus for the PMMA used in our molding process (2.0 mm thick Cast Acrylic, RS Component), a Hounsfield tensile tester was used to collect the stress-strain data, and a Minolta spot thermometer was used to measure the surface temperature of the PMMA specimen. The load-displacement relationships for a typical PMMA specimen at various temperatures are shown in Fig. 1. From the figure, we observed that the PMMA is in glassy state when temperature is below 102 °C, rubbery state when temperature is above this temperature. We can conclude that this PMMA specimen has the glass transition temperature at 102 °C. From those experimental data, we can calculate the Young's modulus as a forth order polynomial function of temperature, as shown in Fig. 2 and Eq. (1):

$$\log E(T) = -1.3909 \times 10^{-7} T^4 + 6.5716 \times 10^{-5} T^3 - 0.0107 T^2 + 0.6707 T - 4.9704 \quad (1)$$

where E is Young modulus (MPa), and T is temperature (°C). These experimental parameters allowed us to determine the Young's modulus of our PMMA substrates at different temperatures during the hot-embossing process. This expression is also useful in calculating the strain and displacement field once the stress field is known, as will be presented in the next section.

3 Modeling hot-embossing by contact stress analysis

Although the hot-embossing process is a proven replication technique, one of its shortcomings is the difficulty of transferring sharp and straight wall features from a mold to a polymer substrate as in Fig. 3. This is mainly due to

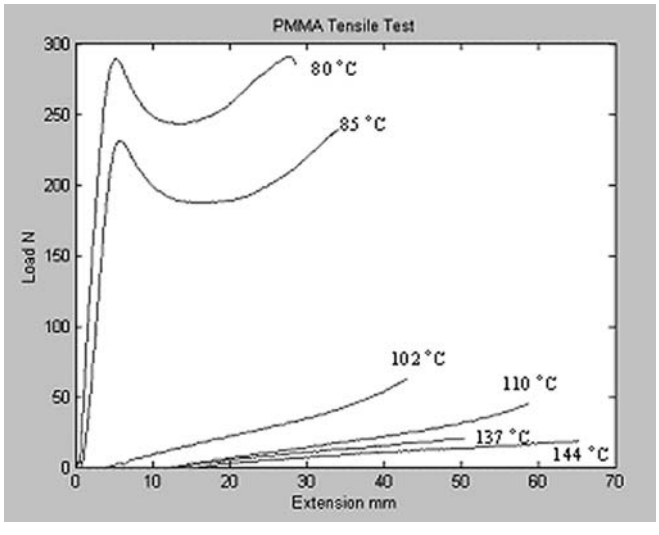

Fig. 1. PMMA tensile test result (Load vs. Extension) under different temperature conditions

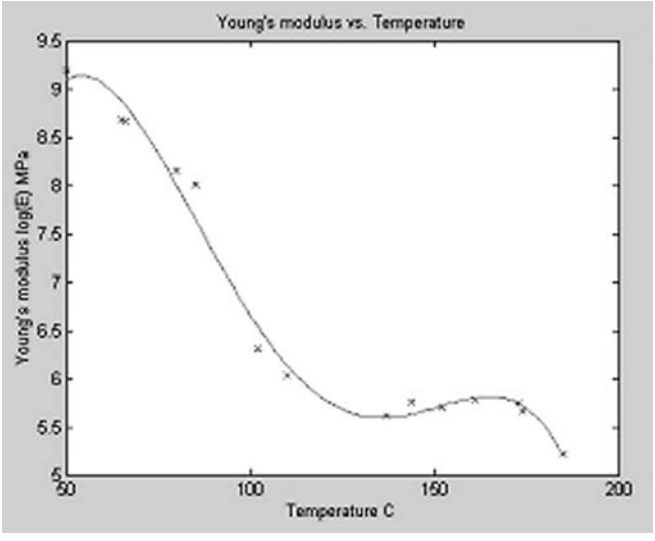

Fig. 2. Experimental relationship between Young's modulus and temperature of PMMA samples

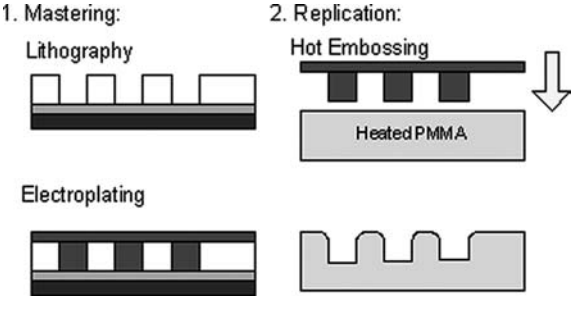

Fig. 3. Fabrication process of the micro molding technique: Lithography, Electroplating, and Hot Embossing. However, the resulting channels may not have straight walls

the contact-stress caused by the mold on a substrate. In this regard, we apply the contact-stress analysis [7] to model the cross sectional profile of microchannels on polymer substrates after the hot-embossing process. Referring to Fig. 4, let p be a contact stress acting over an infinitesimal surface area tdy_1. Then, at an isolated surface at a distance r with unit t, the net force $P = pdy_1$, which yields the following expressions for the radial stresses:

$$\sigma_r = -\frac{2}{\pi r} pdy_1 \cos\theta, \quad \sigma_\theta = 0, \quad \tau_{r\theta} = 0 \tag{2}$$

Note that these stresses satisfy the boundary condition that the net force P must balance the sum of the resultant forces acting on a cylindrical surface of radius r, i.e.:

$$2\int_0^{\pi/2} \sigma_r \cos\theta \cdot r d\theta = -\frac{4P}{\pi}\int_0^{\pi/2} \cos^2\theta d\theta = -P \tag{3}$$

The stresses with respect to the Cartesian coordinate are then represented by

$$\sigma_x = \sigma_r \cos^2\theta = -\frac{2}{}pdy_1 \cos^3\theta$$

$$\sigma_y = \sigma_r \sin^2\theta = -\frac{2}{\pi r} pdy_1 \sin^2\theta\cos\theta$$

$$\tau_{xy} = \sigma_r \sin\theta\cos\theta = -\frac{2}{\pi r} pdy_1 \sin\theta\cos^2\theta \tag{4}$$

Furthermore, expressing r and θ in terms of x and y,

$$r = \sqrt{x^2+y^2}, \quad \cos\theta = \frac{x}{\sqrt{x^2+y^2}}, \quad \sin\theta = \frac{y}{\sqrt{x^2+y^2}}$$

can put in Eq. (4), we have

$$\sigma_x = -\frac{2}{\pi} pdy_1 \frac{x^3}{(x^2+y^2)^2}$$

$$\sigma_y = -\frac{2}{\pi} pdy_1 \frac{xy^2}{(x^2+y^2)^2}$$

$$\tau_{xy} = -\frac{2}{\pi} pdy_1 \frac{x^2 y}{(x^2+y^2)^2} \tag{5}$$

With (5) a contact stress p acting on an area a distance y_1 away from the origin of the coordinate frame as depicted in Fig. 5 would yield the following local stresses at location (x, y)

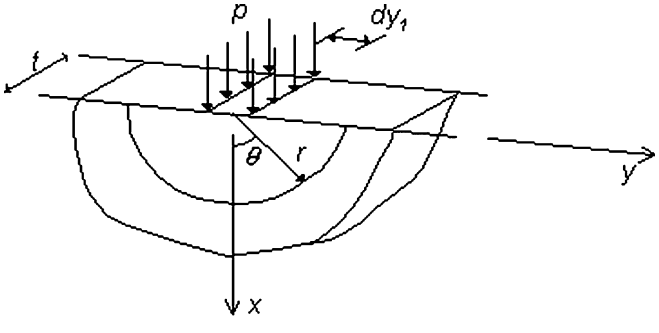

Fig. 4. Free body diagram of a contact stress p acting on origin

$$\sigma_x = -\frac{2}{\pi} pdy_1 \frac{x^3}{[x^2+(y-y_1)^2]^2}$$

$$\sigma_y = -\frac{2}{\pi} pdy_1 \frac{xy^2}{[x^2+(y-y_1)^2]^2}$$

$$\tau_{xy} = -\frac{2}{\pi} pdy_1 \frac{x^2 y}{[x^2+(y-y_1)^2]^2} \tag{6}$$

Now, consider the hot embossing process, where the contact force from the hydraulic press is uniformly distributed over the polymer substrate as in Fig. 6a. The stress distribution from a microchannel mold feature on the substrate is assumed to be a constant pressure distribution $p(y_1) = p_o$ in the region $-a \le y \le a$ as in Fig. 6b. Integration of σ_x for y_1 from $-a$ to a then yields the overall stress experienced at location (x, y) due to the metal mold:

$$\sigma_x = -\frac{2}{\pi} p_o x^3 \int_{-a}^{a} \frac{dy_1}{[x^2+(y-y_1)^2]^2} \tag{7}$$

or letting $u = y - y_1$, one obtains

$$\sigma_x = \frac{2}{\pi} p_o x \left[\frac{u}{2(x^2+u^2)} + \frac{1}{2x}\tan^{-1}\frac{u}{x}\right]_{y+a}^{y-a} \tag{8}$$

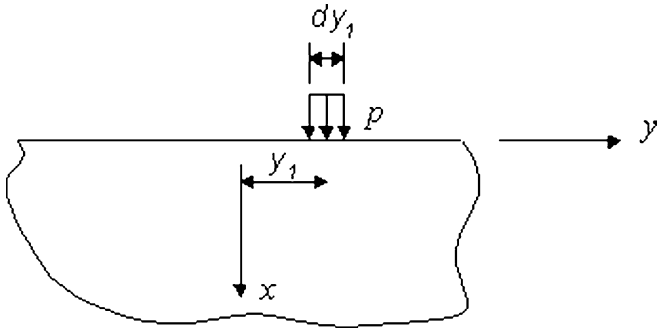

Fig. 5. Free body diagram of a contact stress p acting on right shifting from the origin

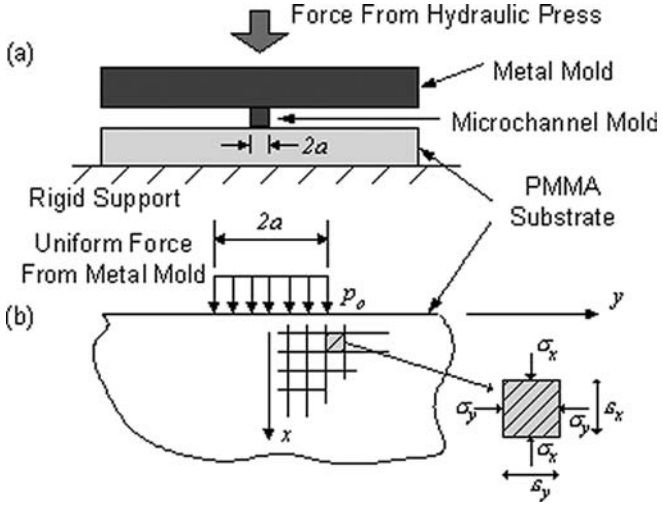

Fig. 6. (**a**) Schematic drawing of hot embossing process using a micro channel mold. (**b**) Free body diagram of PMMA under a force by a mold and rigid support

After substituting the limits of integration and simplifying the resulting equations, and similarly for σ_x and τ_{xy}, one has

$$\sigma_x = \frac{p_o}{\pi}\left\{\frac{2ax(y^2 - x^2 - a^2)}{[x^2 + (y-a)^2][x^2 + (y+a)^2]} + \tan^{-1}\left(\frac{y-a}{x}\right) - \tan^{-1}\left(\frac{y+a}{x}\right)\right\}$$

$$\sigma_y = \frac{p_o}{\pi}\left\{\frac{2ax(x^2 + a^2 - y^2)}{[x^2 + (y-a)^2][x^2 + (y+a)^2]} + \tan^{-1}\left(\frac{y-a}{x}\right) - \tan^{-1}\left(\frac{y+a}{x}\right)\right\}$$

$$\tau_{xy} = -\frac{4p_o}{\pi}\frac{ax^2y}{[x^2 + (y-a)^2][x^2 + (y+a)^2]} \quad (9)$$

With the known stresses and that the substrate is in elastic region, Hooke's law can be applied to calculate the strains. Note that from Fig. 1, when the polymer substrate is above glass transition temperature, it becomes rubbery and does not have a plastic stress-strain region, so these equations can still be used. The strains are related to the Young's modulus E, Poisson ratio ν, and the stresses by the following:

$$\varepsilon_x = \frac{1}{E}(\sigma_x - \nu\sigma_y), \quad \varepsilon_y = \frac{1}{E}(-\nu\sigma_x + \sigma_y) \quad (10)$$

Integrating the strain by substrate thickness, the displacement δ can thus be obtained.

$$\delta_x = \int \varepsilon_x dx \quad (11)$$

The Young's modulus E here is temperature dependent as in equation (1).

The contact-stress analysis allows the deformation of the polymer substrate surface after it is subjected to the hot-embossing process to be modeled. In the next section, prediction from Eq. (11) will be compared with the experimental results.

4 Experimental validation

The contact-stress analysis above assumes a hot-embossing process in which a PMMA substrate is heated above its glass transition temperature and embossed by a metal mold with micro-features. During this process, PMMA substrate is in elastic region ($T > 102°C$ from Fig. 1) and under a uniform distributed contact pressure. The contact-stress analysis subsequently yields expressions for a 2D stress and strain field (Eqs. (9) and (11)) on a polymer substrate due to a uniform contact pressure field p_o applied over an infinitesimal surface area *2a*.

For the validating experiments here, a PMMA substrate was embossed at 120 °C to obtain microchannels of different widths, as shown in Fig. 7. The figure also shows the situation of transferring a sharp and straight wall features to the PMMA substrate. From the contact-stress analysis, the deformation of the PMMA would be dependent on the applied pressure and temperature. Various experiments are hence conducted to compare the microchannel cross sectional profiles between the numerical prediction of the contact-stress analysis and experimental data under different pressure, temperature, and channel width settings. The microchannel profiles were measured by an Alpha-step profiler.

4.1 Different pressures, same temperature and channel width

PMMA substrates were embossed at 120 °C under different pressures. The channel width is 1000 μm. Comparison of numerical prediction from contact-stress analysis and experimental data is given in Fig. 8 for different pressure. The applied pressures were not measured directly but estimated from the numerical prediction to be 19×10^6 N/m^2 and 3×10^6 N/m^2 for the top and bottom plots. The figure indicates that different channel depths can be fabricated with different pressures.

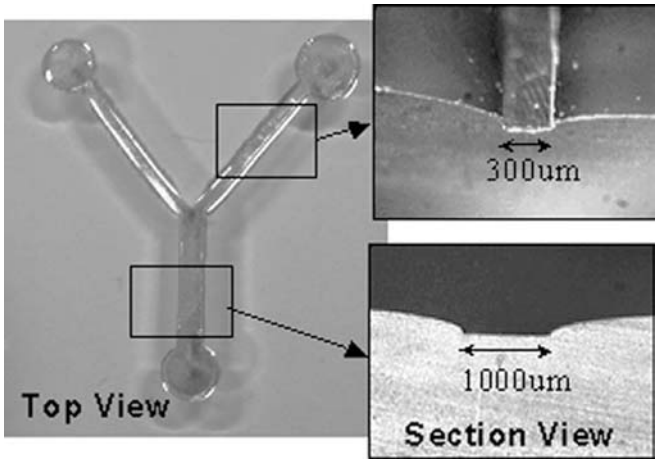

Fig. 7. 3D microscope pictures of a PMMA molded with microchannels using hot-embossing process. As shown in the insets on the right, the channel walls are curved due to contact-stress between the mold and PMMA

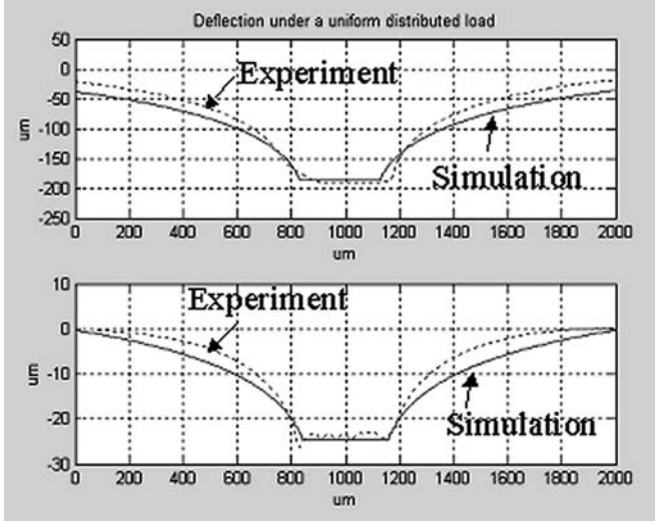

Fig. 8. Comparisons of numerical prediction (solid line) and experimental (dotted line) channe l cross-sectional profile for channels compressed at different pressures with the same width at 120 °C

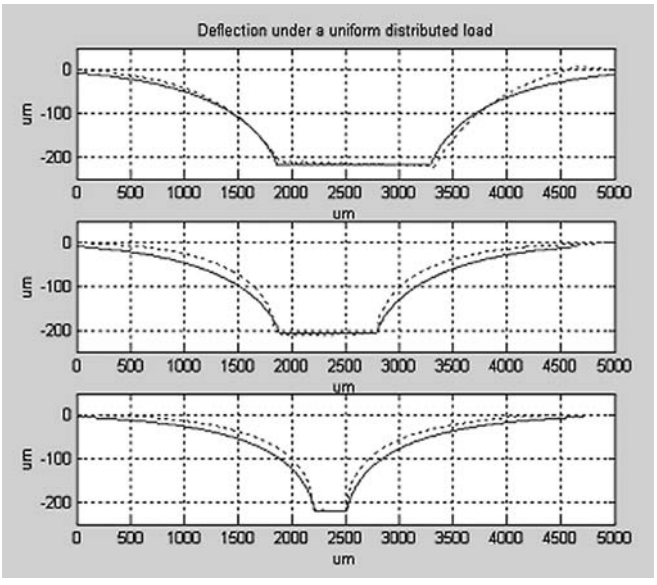

Fig. 9. Comparisons of numerical prediction (solid line) and experimental (dotted line) channel cross-sectional profile for channels compressed at different channel width s under same pressure at 120 °C

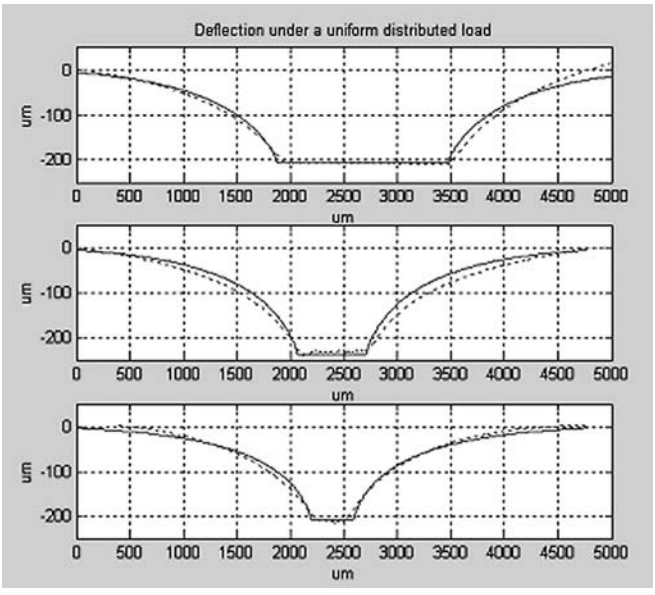

Fig. 10. Comparisons of numerical prediction (solid line) and experimental (dotted line) channel cross-sectional profile for channels compressed at different channel width s under same pressure at 150 °C

4.2
Different channel widths, same pressure and temperature

PMMA substrates were embossed at 120 °C under same pressure but with different channel width (1500 μm, 1000 μm, and 300 μm). The comparison of numerical prediction and experimental data is given in Fig. 9. The applied pressure is estimated to be 18×10^6 N/m^2 in this case. The figure shows that different channel widths can be fabricated with rough the same depth with the same pressure.

4.3
Different channel widths, same pressure, different temperature

PMMA substrates were embossed at 150 °C under the same pressure and different channel width (1500 μm, 1000 μm, and 300 μm). Comparison of numerical prediction and experimental data is given in Fig. 10. Figure 10 is actually not much different from Fig. 9 as Young's modulus varies in a small range when PMMA is above glass transition temperature. The pressure in this case is estimated to be 18×10^6 N/m^2 and is the same as before.

Results from Fig. 8, Fig. 9 and Fig. 10 also indicate a reasonable match between the numerical prediction of contact-stress analysis and the experimental data.

5
Conclusion

Hot-embossing process is a flexible and low-cost microfabrication method for building high aspect ratio polymer based microchannels. However, it is difficult to fabricate sharp and straight wall profile via hot-embossing the PMMA mainly because of the limitation of its physical properties. A quantifying method on the deformation of wall profile during hot-embossing process is thus desired. The present paper shows that the contact-stress analysis for strain displacement can be applied for such purpose. The paper also shows that numerical prediction on wall profiles compare favorably with actual experimental results for channel widths, pressures and temperatures. The present work serves to offer MEMS engineers a tool to predict and design microchannels based on the geometry of micro molds.

References

1. **Linnemann R; Woias P; Senfft CD; Ditterich JA** (1998) A self-priming and bubble-tolerant piezoelectric silicon micropump for liquids and gases, IEEE MEMS 1998 pp 532–537.
2. **Lee GB; Chen SH; Huang GR; Sung WC; Lin YH** (2001) Microfabricated plastic chips by hot embossing methods and their applications for DNA separation and detection, Sensors and Actuators B 75: 142–148.
3. **Olsson A; Larsson O; Holm J; Lundbladh L; Ohman O; Stemme G** (1997) Valve-less diffuser micropumps fabricated using thermoplastic replication, IEEE MEMS 1997, 305–310.
4. **Li Chong VKW; Lei KF; Li WJ Lee T** (2003) Development of mass-manufacturable micro/nano fluidic devices using standard CD fabricatin technology, The 1st International Meeting On Microsensors and Microsystems (2003), January 12–14.
5. **Lei KF; Li WJ; Budraa N; Mai JD** (2003) Microwave bonding of polymer-based substrates for micro/nano fluidic applications, The 12th International Conference on Solid-State Sensors, Actuators, and Microsystems (Transducers 03'), June 8–12.
6. **Brydson J** (1999) Plastics Materials Butterworth Heinemann 43–75.
7. **Budynas RG** (1999) Advanced Strength and applied Stress Analysis McGraw-Hill 358–361.